Precambrian Research 359 (2021) 106212

Contents lists available at ScienceDirect

Precambrian Research

journal homepage: www.elsevier.com/locate/precamres

Constraining the Cambrian drift of Gondwana with new paleomagnetic data from post-collisional plutons of the Araçuaí orogen, SE Brazil

F.A. Temporim [a,b,*], U.D. Bellon [a], M. Domeier [b], R.I.F. Trindade [a], M.S. D'Agrella-Filho [a], E. Tohver [a]

[a] Instituto de Astronomia, Geofísica e Ciências Atmosféricas (IAG), Departamento de Geofísica, Universidade de São Paulo, São Paulo, Brazil
[b] Centre for Earth Evolution and Dynamics (CEED), University of Oslo, Oslo, Norway

ARTICLE INFO

Keywords:
Paleomagnetism
Western Gondwana
Cambrian
Araçuaí Orogen
Thermal diffusion model

ABSTRACT

Despite their importance in constraining the dynamics of Gondwana's final phase of assembly, Cambrian paleomagnetic data from Gondwana are sparse. The Cambrian paleomagnetic dataset of Western Gondwana is especially poor, being defined by only a handful of poles. Here we contribute new Furongian paleomagnetic data from the ~500 Ma post-collisional, Santa Angelica and Venda Nova plutons from the southern portion of the Araçuaí orogen in SE Brazil. The characteristic magnetization isolated from both plutons reveals two groups of directions that are demonstrated to be antipodal. On the basis of a thermal diffusion model, we attribute these antipodal directions to primary thermoremanent magnetizations acquired by cooling of the plutons in the presence of a reversing field. Together, paleomagnetic results from 35 sites distributed between the two plutons allows computation of a new ~500 Ma paleopole: 4.7° N, 332.2° E, $A_{95} = 4.06$ and $K = 68.82$. This pole does not resemble any younger paleomagnetic poles either from Gondwana or the independent South American plate after the demise of Pangea, but instead closely corresponds to the Miaolingian and Furongian sector of reference apparent polar wander paths for Gondwana. It also agrees well with the limited existing individual early Paleozoic poles from Western Gondwana. Our new result may thus be regarded as a reference pole for Western Gondwana in Furongian time. Considerations of the Cambrian paleomagnetic data from Eastern and Western Gondwana suggest that while the supercontinent was amalgamated by ~500 Ma, there was likely significant motion between Eastern and Western Gondwana in earlier Cambrian time.

1. Introduction

Gondwana was the largest continental crustal unit on Earth for over 200 million years (Meert and Van der Voo, 1997). This supercontinent comprised the current African continent, Madagascar, India, Arabia, and much of southwestern Europe, South America, Antarctica, Australia (Torsvik and Cocks, 2011), as well as many smaller units such as Florida, the Taurides of Turkey, and parts of central Asia and China (Torsvik and Cocks, 2016). Following the breakup of preceding supercontinental assemblies (Meert and Van der Voo, 1997), Gondwana was generated through a series of major orogenic events, including the East African and Brasiliano-Pan-African events, which marked the closure of Neoproterozoic oceans (Kröner and Stern, 2005). The East African orogeny started the process between 800 and 650 Ma (Wilson et al., 1997), but the subsequent evolution of Gondwana remains somewhat unclear. Although the bulk of the supercontinent is generally considered to have been assembled by ca. 550 Ma (Meert and Van der Voo, 1997), some important cratonic elements (e.g. Amazonia, West Africa) may not have fully amalgamated with central Gondwana until the Cambrian Epoch 2–Furongian (Trindade et al., 2006; Tohver et al., 2012), although an early amalgamation, at 650–600 Ma, is also advocated (e.g., Granade de Araujo et al., 2014). Some terranes (e.g. Avalonian and Armonian Terrane Assemblage) along the eastern flank of the Appalachian–Caledonian orogen, were separated from Gondwana in the Late Cambrian (Furongian) and Lower Ordovician (Tremadocian) (Torsvik and Cocks, 2016). To reach a full understanding of this key terminal phase of Gondwana's assembly will require additional paleogeographic constraints.

Continental paleogeography can be derived from paleomagnetic studies that can determine the latitude and orientation of a given continent with respect to the spin axis of the Earth (Torsvik et al., 2012). However, there is a scarcity of high-quality paleomagnetic data of

* Corresponding author at: Rua do Matão, 1226 Cidade Universitária São Paulo, SP 05508-090, Brazil.
E-mail address: filipeat@iag.usp.br (F.A. Temporim).

https://doi.org/10.1016/j.precamres.2021.106212
Received 29 December 2020; Received in revised form 29 March 2021; Accepted 30 March 2021
Available online 19 April 2021

Cambrian age from Gondwana, resulting in persisting uncertainties concerning global paleogeography at this time (Tohver et al., 2006; Li et al., 2013). Here we work to rectify this deficiency through the presentation of a high-quality paleomagnetic pole obtained from Furongian post-collisional plutons of the Araçuaí orogen, SE Brazil. Together with the existing data from Gondwana, we use this new result to constrain the Furongian-Tremadocian drift of Gondwana.

2. Regional geology of the post-collisional pluton from the Araçuaí orogen

The Ribeira, Araçuaí, and Western Congo belts form an orogenic system ~500 km wide and >1000 km long resulting from the Brasiliano-Pan-African event, and represent the final amalgamation of the Gondwana supercontinent (Fig. 1A) (Pedrosa-Soares et al., 2001; Alkmim et al., 2006; Tedeschi et al., 2016). This Neoproterozoic-Cambrian Orogen is contained in a great recess delineated on three sides by ancient, crystalline basement rocks of the São Francisco and Congo cratons. The Araçuaí orogen (AO) merges to the south with the coastal Ribeira orogen, forming the Araçuaí-Ribeira orogenic system (AROS) (Tedeschi et al., 2016) (Fig. 1A).

Different magmatic supersuites following the typical geochemical and structural evolution of collisional settings have been recognized in the region (Pedrosa-Soares et al., 2011), comprising: (i) a pre-collisional G1 supersuite, represented by the Rio Doce magmatic arc (630–585 Ma); (ii) a *syn*-collisional G2 supersuite, represented by garnet-bearing leucogranites (585–560 Ma); (iii) a late-collisional G3 supersuite comprising mostly leucogranites (560–535 Ma); and (iv) post-collisional supersuites G4 and G5 (530–480 Ma). This last phase is inferred to relate to the gravitational collapse of the orogen, leading to an extensional regime at the end of the Brasiliano Orogeny. In the north, Cambrian post-collisional plutons form large, elongated N-striking bodies parallel to the belt (Fig. 1A). In the south, the volume of post-collisional magma was significantly lower and the intrusions are mostly circular in shape (Fig. 1A). These plutons mostly include I-type and A-type granitic rocks, and their Opx-bearing charnockitic equivalents (Pedrosa-Soares and Wiedemann-Leonardos, 2000; De Campos et al., 2016). Usually they form inversely-zoned, balloon-like plutons, composed of granitic-charnockitic rocks and gabbronoritic cores, with striking magma mixing and mingling features, and chemical-isotopic evidence of mantle

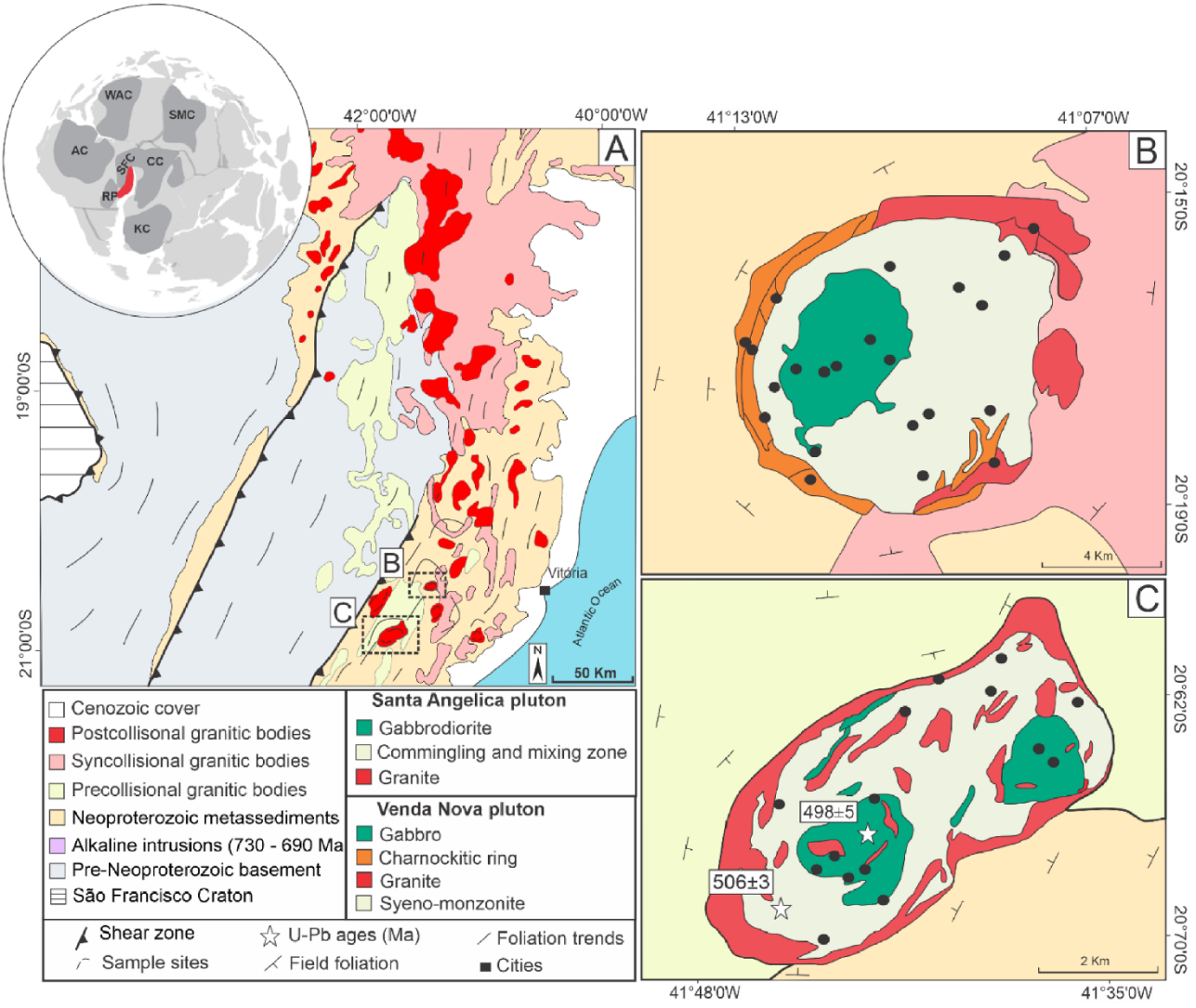

Fig. 1. (A) Simplified geological map of the Araçuaí orogenic system (the red inset shows the location of the Araçuaí-Ribeira orogen in Western Gondwana) (modified from Pedrosa-Soares and Wiedemann-Leonardos, 2000). (B) Geological map with facies distribution for Venda Nova (VN) pluton and country rocks (Mendes and De Campos, 2012). (C) Geological map with facies distribution for Santa Angélica (SA) pluton and country rocks (modified from Schmidt-Thomé and Weber-Diefenbach, 1987). Paleomagnetic sampling sites are denoted with black dots. Stars represent U-Pb analyses from SA (Temporim et al., 2020). AC: Amazonian Craton; CC: Congo Craton; KC: Kalahari Craton; RP: Rio de la Plata Craton; SFC: São Francisco Craton; SMC: Sahara Meta-Craton; WAC: West African Craton.

involvement (De Campos et al., 2016) (Fig. 1B,C). No tectonic movement is recorded after this phase in the AO, therefore the post-collisional plutons from the south do not show evidence of displacement (De Campos et al., 2016, Temporim et al., 2020).

The Venda Nova (VN) pluton corresponds to an elliptical structure with a ~75 km^2 area (Fig. 1B) and concentric structures arrayed about the whole body (Mendes and De Campos, 2012). The country rocks are biotite-garnet-sillimanite gneisses and orthogneisses. Gradual contacts are subvertical and the foliation of the pluton is parallel to the contact with the country rocks and it dips towards the interior of the intrusion (Mendes and De Campos, 2012). The VN pluton is inversely zoned with a felsic border and mafic core. It exhibits a gabbro-norite core, a chanockitic ring at the western border, and a syeno-monzonite envelope and monzodiorite in the interior of the pluton, as a result of commingling between the syeno-monzonite and gabbro-norite units (Mendes and De Campos, 2012).

The Santa Angelica (SA) pluton (Fig. 1C) covers about 200 km^2 and is an elliptical-shaped intrusion elongated along a NE-SW axis and with concentric structures arrayed about a twin, bulÍs eye pattern (De Campos et al., 2016; Temporim et al., 2020). The country rocks are biotite-garnet-sillimanite gneisses and biotite-hornblende granodioritic to tonalitic gneisses. Gradual contacts between the intrusion and the country rock are subvertical and the foliation at the border of the pluton is parallel to the contact with the country rocks (De Campos et al., 2016), dipping towards the interior of the intrusion. The SA pluton is also inversely zoned with felsic rocks at the borders and more intermediate-mafic rocks towards the cores of the twin intrusions (Schmidt-Thomé and Weber-Diefenbach, 1987). The commingling and mixing zones are defined through field and geochemical data by Bayer et al. (1987). Hybrid rocks, resulting from commingling of basic and acidic magmas are widespread in the intrusion. U-Pb zircon ages constrain the crystallization age of different suites within the SA: 506 ± 3 Ma for the felsic border and 498 ± 5 Ma for the mafic core (Temporim et al., 2020).

3. Paleomagnetism

3.1. Sampling and methods

Paleomagnetic samples were collected from multiple rock types from both VN (22 sites) and SA (15 sites) (Fig. 1B,C). Between five and seven cores of approximately 8 cm in length and 2.5 cm in diameter were collected at each site using a portable gasoline-powered drill. The cores were oriented in the field by sun and magnetic compasses. In the laboratory, samples were cut into 22 × 25 mm cylindrical specimens and submitted to thermal (TH) or alternating field (AF) demagnetization. Paleomagnetic analyses were performed in the Laboratório de Paleomagnetismo of the Universidade de São Paulo (USPmag). Remanent magnetizations were measured with a 2G-Enterprises SQUID magnetometer. AF demagnetizations were executed with an automated three-axis AF-demagnetizer coupled with the magnetometer. TH demagnetizations were performed with an ASC TD48SC paleomagnetic oven (peak temperatures within ±5 °C). These instruments are housed in a magnetically shielded room with ambient field <500 nT. Magnetic components for each specimen were identified in orthogonal plots and calculated through principal component analysis (PCA) (Kirschvink, 1980). Vector mean directions were computed using standard Fisher statistics (Fisher, 1953).

A total of 127 specimens from the SA pluton and 198 specimens from the VN pluton were analyzed. After measuring their natural remanent magnetization (NRM), two specimens from each site were submitted to AF demagnetization with steps of 1 mT (1–10 mT), 2 mT (10–20 mT), 5 mT (20–50 mT) and 10 mT (50–100 mT), and two other specimens were submitted to TH with steps of 50 °C (100–500 °C), 20 °C (500–560 °C), 10 °C (560–580 °C) and 20 °C (580–680 °C). AF demagnetization was then applied to all sites where AF demagnetization was effective. For all remaining sites (for which AF demagnetization was not adequate alone), demagnetization followed a combination of two steps: AF demagnetization at 5 and 10 mT to suppress the contribution of MD magnetite, and then complete TH demagnetization with the steps described above.

A series of rock magnetic experiments were executed to investigate the magnetic mineralogy to better understand the paleomagnetic results. Thermomagnetic experiments were conducted under argon flux to prevent excessive oxidation during heating using a CS-2 furnace attached to an Agico Kappabridge KLY 4 CS. All thermomagnetic K-T curves (susceptibility vs. temperature) were determined in the temperature interval from −200 to 700 °C. Isothermal remanent magnetization (IRM) curves and hysteresis curves were obtained with a vibrating sample magnetometer (VSM) MicroMag 3900 (Princeton Measurements Corp).

3.2. Paleomagnetic results

K-T curves, magnetic hysteresis and IRMs were measured on several samples from each lithology of the SA and VN plutons to characterize the magnetic mineralogy. All facies have almost the same behavior, as showed by Temporim et al, (2020). Hence, the results from one sample from each pluton are presented in Fig. 2.

The K-T curves of all samples exhibit major transitions (identified from the derivative of the curves, i.e. dK/dT) at −169.3 °C and 578.6 °C for SA, and at −168.9 °C and 566.3 °C for VN pluton, interpreted as the Verwey Transition (VT) and the magnetite Curie Temperature (MCT), respectively (Fig. 2A). Magnetic hysteresis (Fig. 2B) of the samples reveal similar Mrs/Ms relations and a high Hcr/Hc, with thin hysteresis, typical of an assemblage dominated by multidomain (MD) magnetite. IRMs (Fig. 2C) show quick saturation around 0.1 T and an Hcr smaller than 20 mT. These results suggest that magnetite is the main carrier of the magnetic remanence in both the SA and VN plutons, and that some of the magnetite occurs in the form of MD grains. The presence of such MD magnetite is of concern since it can acquire a remanence at relatively low temperatures, but may survive TH treatment up to 450 °C, and can thus obscure the remanent magnetizations carried by pseudo-single and single domain magnetite (Dunlop and Argyle, 1991). To address this problem, all specimens subjected to TH demagnetization were first subjected to AF of 5 and 10 mT to suppress any contributions from MD magnetite. A typical example of the success of this approach can be seen in sample SA43D2 (Fig. 3).

With demagnetization, individual samples exhibited a variety of magnetization unblocking behaviors. Some samples exhibited unstable behavior during demagnetization with no well-defined linear segments or great-circle trajectories and so were excluded from further analysis. All other paleomagnetic results from the VN and SA plutons are summarized in Table 1. Characteristic AF and TH demagnetization results are depicted in Fig. 3. AF demagnetization proved effective for almost all sites (Fig. 3), and the complete demagnetization of most samples was attained at relatively high peak fields between 40 and 100 mT (Fig. 3). Some sites were not completely demagnetized by AF and TH demagnetization was necessary (SA40 and VN9). In these cases, demagnetization was generally characterized by 'hard-shouldered' behavior, with unblocking mostly occurring within a narrow range of temperatures between 540 and 580 °C (e.g. SA40A3, VN7D2, VN9G2 and VN25C1 in Fig. 3). However, both methods of demagnetization resulted in similar directional data (Fig. 3). The most common behavior observed during demagnetization was dual-component decay, with a low coercivity/temperature component being eliminated before reaching a stable high temperature or high coercivity direction (e.g. SA43 in Fig. 3). In these samples, the low-stability component was removed during the initial steps of demagnetization (5–20 mT or 100–150 °C), and its remanence is probably carried by coarse-grained MD grains. After removal of the low-stability component, the magnetic vector proceeds univectorially to the origin, allowing definition of the characteristic remanent magnetization (ChRM).

The ChRMs of both the VN and SA plutons present two groups of

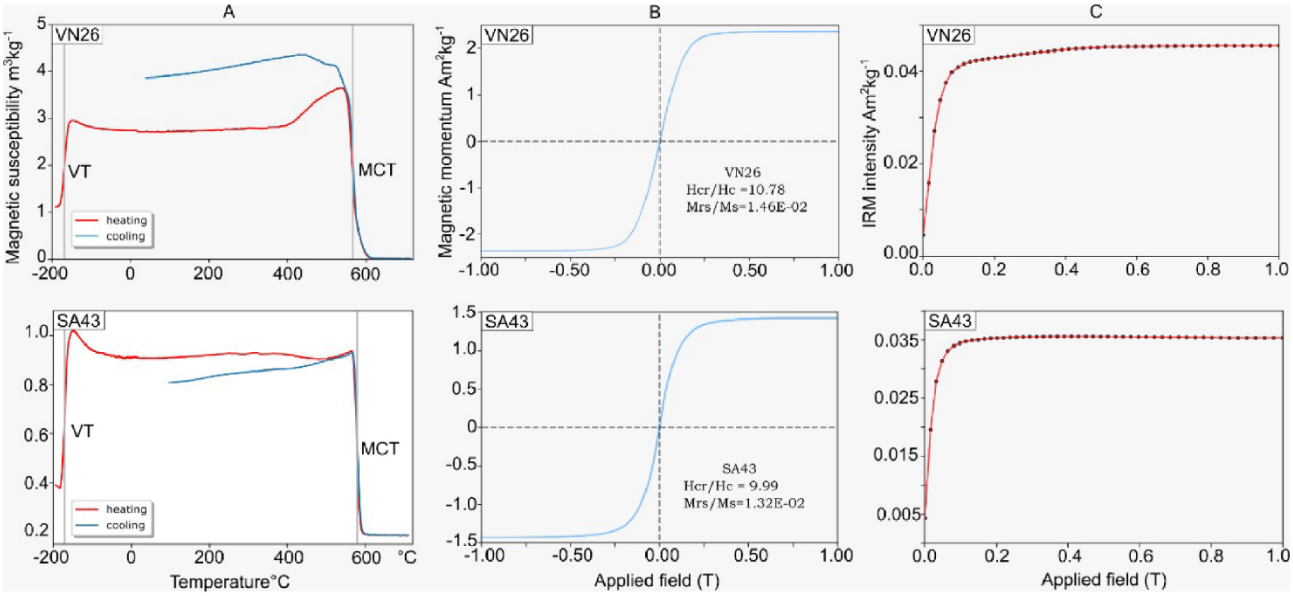

Fig. 2. Investigations of the magnetic mineralogy of the Venda Nova (VN) and Santa Angélica (SA) plutons. A- thermomagnetic curves for gabbroic rocks of VN and SA showing the Verwey transition (VT) and magnetite Curie temperature (MCT). B- Magnetic hysteresis and C- Isothermal remanence magnetization (IRM) acquisition curves. Hcr: remanence coercivity, Hc: bulk coercivity, Mrs: saturation remanent magnetization, Ms: saturation magnetization.

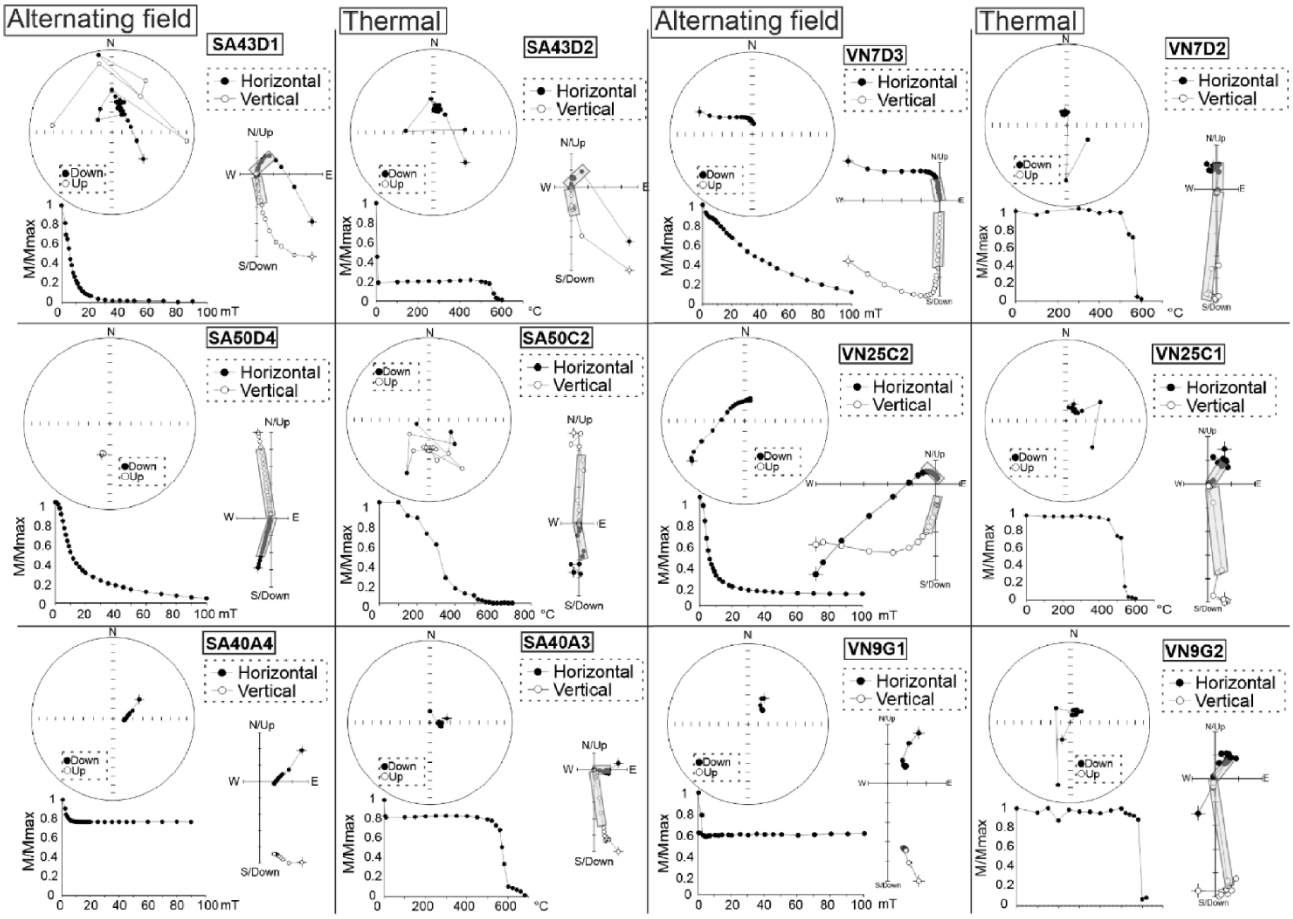

Fig. 3. Typical alternating field and thermal demagnetization results for Santa Angélica (SA) and Venda Nova (VN) pluton, shown as orthogonal and stereographic projections and magnetization intensity decay curves. Open (full) symbols correspond to negative (positive) inclinations in the stereographic projections.

Table 1
Paleomagnetic results for SA and VN plutons. The mean ChRM is given by its declination (Dec), inclination (Inc), radius of the 95% confidence cone (α95), and precision parameter (K). N/n indicates number of samples collected/used in calculation of the mean. VGP Plat/Plong indicates virtual geomagnetic pole coordinates.

Site#	N/m	Geographical coordinates	Site mean direction					VGP	
		Lat. (S)	Long. (W)	Dec (°)	Inc (°)	α_{95}	K	Plong.(°E)	Plat.(°N)
Santa Angélica pluton									
SA23	6/6	20° 41′ 57.902″	41° 26′ 54.866″	354.5	55.0	14.6	22.12	227.7	55.1
SA34	6/6	20° 43′ 39.204″	41° 26′ 42.743″	76.2	60.8	6.2	116.66	84.2	59.6
SA37	12/8	20° 42′ 39.409″	41° 25′ 37.141″	46.2	75.1	3.0	352.45	30.4	83.2
SA38	8/8	20° 42′ 17.245″	41° 26′ 25.051″	65.1	83.5	5.5	103.17	357.7	68.3
SA40	10/10	20° 42′ 6.591″	41° 25′ 59.143″	65.8	78.6	2.7	328.71	21.5	73.1
SA42	9/8	20° 41′ 40.204″	41° 26′ 32.991″	45.3	59.1	10.6	28.04	135.7	70.6
SA43	13/13	20° 40′ 37.939″	41° 25′ 47.953″	19	69.2	11.7	13.46	226.7	79.5
SA44	10/7	20° 40′ 22.646″	20° 40′ 22.646″	359.4	66.7	11.2	29.95	242.7	67.5
SA49	8/8	20° 39′ 55.802″	41° 21′ 52.343″	17.8	61.6	14.1	16.4	202.7	71.3
SA50	8/8	20° 39′ 44.341″	41° 22′ 22.077″	182.8	−59.4	3.6	243.9	43.2	−62.9
SA53	7/7	20° 38′ 31.818″	41° 21′ 29.632″	191.3	−55.7	9.6	40.40	26.0	−63.2
SA55	8/8	20° 38′ 19.800″	41° 23′ 8.249″	83	74.2	6.3	78.75	43.9	65.9
SA59	11/11	20° 38′ 18.665″	41° 24′ 43.889″	247.4	−76.5	7.3	44.63	214.4	−73.4
SA61	8/8	20° 39′ 5.051″	41° 25′ 18.916″	29.0	78.0	7.0	64.38	325.6	80.7
SA66	11/11	20° 37′ 39.366″	41° 22′ 53.633″	28.7	73.2	4.65	103.13	266.7	86.6
Mean	135/127	20° 40′ 30.000″	41° 25′ 15.600″	29.20	71.37	10.05	15.45	335.4	6.8
Venda Nova pluton									
VN1	8/6	20° 19′ 4.079″	41° 9′ 27.377″	33	72.5	6	124.43	130.0	83.7
VN2	8/6	20° 19′ 10.042″	41° 10′ 26.672″	24.9	70.6	5.8	132.77	169.1	81.6
VN3	10/10	20° 18′ 38.211″	41° 10′ 52.834″	21.1	73.7	3.1	247.07	202.7	85.7
VN4	13/13	20° 18′ 24.871″	41° 10′ 35.416″	21.2	69.4	2.5	277.97	181.4	79.5
VN5	9/9	20° 18′ 57.275″	41° 12′ 17.472″	345.5	79.7	4.4	135.19	294.4	72.7
VN6	8/8	20° 17′ 18.463″	41° 13′ 14.549″	17.9	75.6	6.6	71.09	252.5	86.1
VN7	14/14	20° 17′ 15.302″	41° 13′ 17.743″	356.6	76.7	2.1	345.05	273.5	76.9
VN8	8/7	20° 16′ 36.128″	41° 12′ 56.959″	27	77.3	8.6	50.60	347.8	87.4
VN9	12/12	20° 16′ 3.724″	41° 11′ 4.764″	50.2	71.8	1.9	500.51	91.5	76.6
VN11	14/13	20° 18′ 22.548″	41° 9′ 30.936″	18.5	73.4	3.1	180.19	211.5	84.5
VN15	6/6	20° 15′ 38.447″	41° 9′ 10.300″	30.6	74.8	5.3	158.55	113.2	87.5
VN18	5/5	20° 15′ 23.171″	41° 8′ 43.354″	58.5	73.8	4.8	260.21	71.3	74.6
VN22	11/11	20° 18′ 54.745″	41° 12′ 19.573″	0.8	81.2	4.3	111.66	310.0	76.6
VN23	11/11	20° 17′ 41.426″	41° 12′ 27.597′	20.8	72.5	5.4	73.75	193.7	83.9
VN24	10/10	20° 17′ 48.697″	41° 11′ 54.963″	27.4	80.8	4.6	109.02	345.2	81.1
VN25	11/11	20° 17′ 14.265″	41° 11′ 13.540″	26.2	72.3	2.0	525.36	165.3	84.3
VN26	10/10	20° 17′ 41.009″	41° 11′ 40.622″	22.6	83.3	3.3	209.67	339.7	76.3
VN30	8/8	20° 16′ 37.925″	41° 9′ 33.174″	29.7	73.6	5.6	97.97	139.4	86.1
VN31	9/9	20° 16′ 23.116″	41° 9′ 55.503″	30.8	71.2	3.4	236.65	145.3	82.3
VN33	9/9	20° 17′ 31.640″	41° 10′ 59.414″	59.1	73.4	5.2	100.24	72.9	74
VN35	6/6	20° 19′ 18.177″	41° 12′ 15.183″	21.1	77.8	7.6	78.46	312.3	85.8
VN36	4/4	20° 18′ 25.079″	41° 13′ 4.506″	26.7	77.0	7.4	155.96	345.5	87.9
Mean	204/198	20° 17′ 20.400″	41° 10′ 40.800″	26.74	75.66	3.8	67.44	330.5	3.2
Combined poles									
Mean	37/35	20° 17′ 49.200″	41° 29′ 6.000″	27.84	74.23	4.27	33.15	332.2	4.7

directions: one directed steeply down to the NE (group 1), and a second group directed steeply up to the SW (group 2). In the VN pluton, all sites in the interior of the pluton exhibit group 1 directions, whereas seven sites located at the margin of the pluton present mixed group 1 and 2 directions (Fig. 4A). In the SA pluton, most sites exhibit group 1 directions, but 4 sites in the NE portion of the pluton present group 2 directions or mixed group 1 and 2 directions (Fig. 4B). To consider if the group 1 and group 2 directions could be antipodal (normal and reverse) components of a common population, we executed a test for a common true mean direction (CTMD; Koymans et al., 2016) after inverting the polarity of one of the groups. To consider the uncertainties associated with this test, a non-parametric bootstrap was performed following the approach described by Tauxe et al. (2010). It was not possible to perform this test on the data from the VN pluton because of the large dispersion of the group 2 directions, but application of this test to the data from the SA pluton reveals that the group 1 and group 2 directions are not distinguishable at the 95% confidence level (Fig. 5A). Because these groups are antipodal, this constitutes a positive reversal test. Given this outcome, we interpret the group 1 and group 2 directions to be antipodal directions of a common population, and so treat them together in the following.

To consider whether the VN and SA directional populations may average paleosecular variation (PSV), we employed the approach of Deenen et al. (2011). In this approach, the A_{95} of virtual geomagnetic poles (VGPs) derived from a directional population are evaluated against theoretical bounding values (A_{95min} and A_{95max}) that are dependent on the number of observations (N); A_{95} values that fall between the reference bounding values are considered consistent with a population that has averaged PSV. Converting the site mean ChRM directions from VN to VGPs, we compute a mean paleomagnetic pole of 330.5 °E and 3.2 °N, with an A_{95} of 3.80° (Fig. 4A', Table 1). An interactive cut-off for this VGPs distribution (Vandamme, 1994) of 17.27° did not result in the exclusion of any sites. For N = 22, A_{95max} is 11.70° and A_{95min} is 3.49°, and so our A_{95} of 3.80° falls between these values and is thus consistent with having averaged PSV. For the SA pluton, the site-based VGPs yield a paleomagnetic pole at 335.4 °E and 6.8 °N with an A_{95} of 10.05° (Fig. 4B', Table 1). The interactive cut-off was 32.66°, which again did not result in the exclusion of any sites. For N = 15 the A_{95max} is 14.89° and A_{95min} 4.06°, so again our A_{95} falls within this envelope and is consistent with having averaged PSV.

The CTMD test was used to evaluate whether the VGPs of the VN and SA plutons could belong to the same population. Like the reversal test, the result (Fig. 5B) shows bootstrapped (x,y,z) coordinates for both directional populations as cumulative distribution functions. The

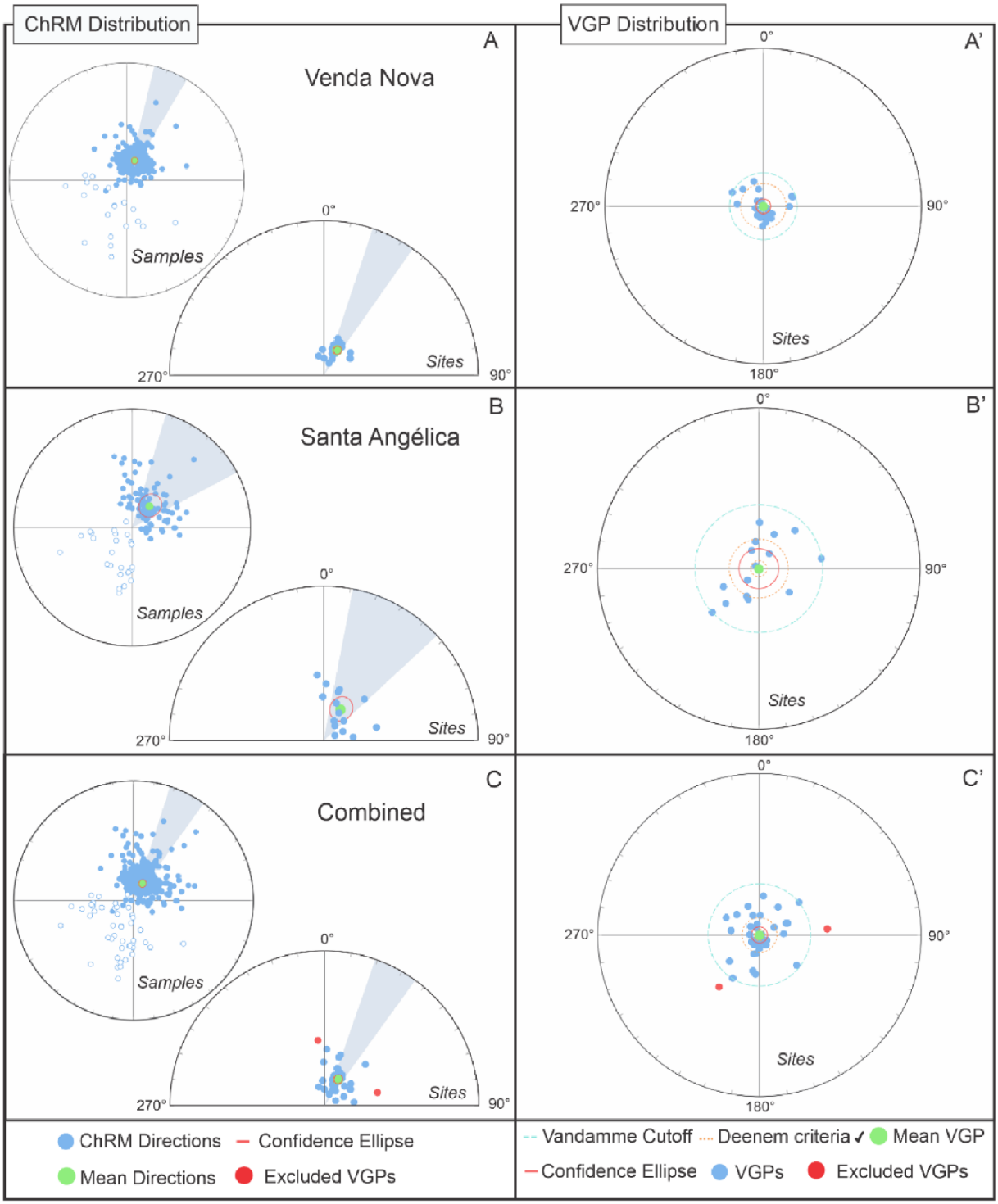

Fig. 4. - Sample and site mean directions for the Santa Angélica (SA) and Venda Nova (VN) plutons and their corresponding VGPs. (A) ChRM directions of the VN samples and their site mean directions; (A') Relative VGP positions with the mean VGP rotated to the north pole. (B) ChRM directions of the SA samples and their site mean directions; (B') Relative VGP positions with the mean VGP rotated to the north pole. (C) ChRM directions of the combined samples and their site mean directions; (C') Relative VGP positions with the mean VGP rotated to the north pole. Filled (open) circles are projections on the lower (upper) hemisphere. Blue points are accepted, and red ones are rejected after a Vandamme cut-off (Vandamme, 1994). The illustrated confidence envelopes show the α95/A95 associated with the mean of the directions/VGPs. All quantitative values are reported in Table 1 of this work.

confidence intervals for each coordinate overlap, indicating that the associated directions are statistically indistinguishable, and thus it can be concluded their populations share a common true mean direction at the 95% confidence level (Koymans et al., 2016). Since the VN and SA plutons are located only tens of kilometers apart, they are part of the same petrological suite, and their VGP populations are statistically indistinguishable, we combine their paleomagnetic data into a single pole. This combination improves the general statistical quality of the pole with a greater N. The combined paleomagnetic pole falls at 332.2° E and 4.7° N, with an A_{95} of 4.06° (Table 1). The interactive cut-off circle for the combined pole was 25.94°, which excluded two sites (Fig. 4C, C'). The observed A_{95} falls between the N = 35 A_{95max} of 8.73° and

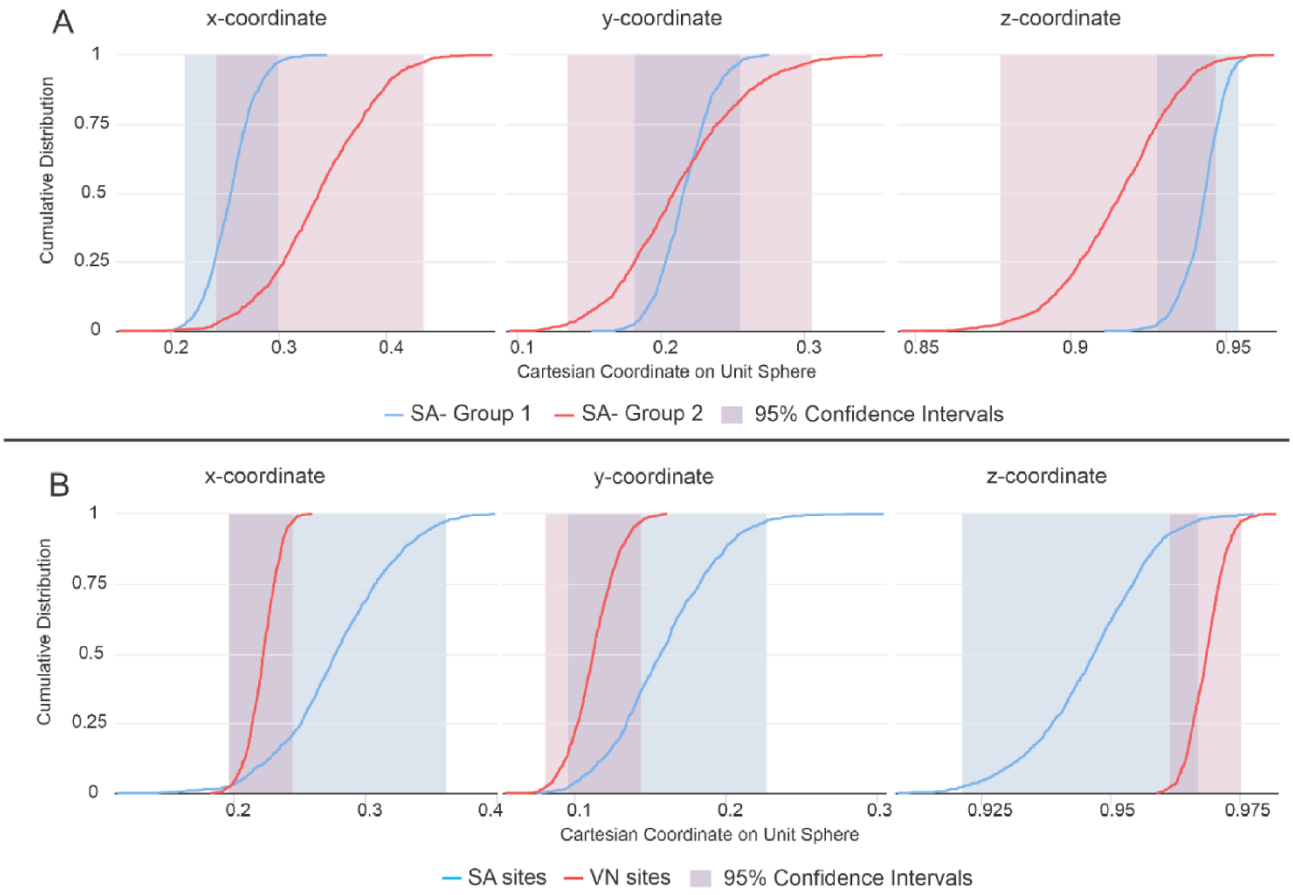

Fig. 5. Common true mean direction (CTMD) test showing the cumulative distribution of Cartesian (x, y, and z) components of the mean directions from non-parametric bootstraps. If the confidence intervals of all components of the two sample sets overlap, they are determined to share a common true mean direction at 95% confidence. (A) CTDM test of the group 1 and 2 ChRMs of the SA pluton. (B) CTDM test of the SA and VN VGPs. Both test results reveal that the populations are indistinguishable at the 95% confidence level.

A_{95min} of 2.89°, again indicating that the combined pole exhibits the dispersion expected from a time-averaged pole.

4. Thermal diffusion model

4.1. Model setup

If the magnetization preserved by the SA and VN plutons is primary, it would represent a thermoremanent magnetization (TRM) acquired during cooling of the plutons below a magnetic blocking temperature. It is therefore important to consider the thermal history of these bodies, and we thus construct a simple thermal diffusion model. To simulate the cooling process of the SA and VN plutons, a two-dimensional heat conservation equation was applied, which takes the form:

$$\left(\frac{dT}{dt}\right) = \kappa\left(\frac{\partial^2 T}{\partial x^2} + \frac{\partial^2 T}{\partial y^2}\right) + H \quad (1)$$

Assuming the term κ (thermal diffusivity) = (k $\rho^{-1}C_p^{-1}$), where ρ is the density of the material (kg m^{-3}), C_p is the thermal capacity at a constant pressure (J/kg/K), k is the thermal conductivity (W/m/K) and H is the volumetric heat production (Wm^{-3}). The terms accompanied by κ are the second derivative of the temperature of the medium, i.e., the temperature variation in the x and y directions. For most mantle and crustal rocks, radioactive heat only becomes relevant at temperatures above 1200 °C (Clauser, 2009), and as such, we ignored the heat production in Eq. (1). As Eq. (1) is a differential equation, it was solved numerically using a finite-difference method in a python script environment. Further details of this thermal diffusion model can be found in the supplementary material.

In the case of the VN pluton, we directly simulated the initial matrix of T_0 (the initial state, i.e., its emplacement) undergoing diffusion for 3 Ma. As proposed by Temporim et al. (2020), the SA pluton consists of two plutonic features, a SW and a NE lobe, separated by an internal magmatic shear zone. Therefore, two different scenarios were proposed for SA: a) these two plutons intrude at the same time with the same T_0 and undergo heat diffusion for 3 Ma; b) the shallowest pluton (the NE lobe) intrudes first, cools down and then the SW pluton intrudes the nearby wall rocks. In scenario (b), the cooling process of the earlier NE pluton and its host was alternatively simulated for 100 kyr and 1 Ma prior to intrusion of the SW pluton, to investigate the differences associated with an approximately coeval intrusion versus a late emplacement. After the intrusion of the SW body, heat diffusion was simulated for an additional 3 Ma.

4.2. Model results

Given the presence of antipodal directions, one way to assess whether the magnetizations could be primary is to consider if the observed spatial distribution of the two polarities could be explained by cooling of the plutons. Thus, our thermal diffusion model can here serve as a kind of field stability test (Van der Voo, 1990; Meert et al., 2020). As discussed below, the results of our model indeed demonstrate that the spatial distribution of magnetic polarity can be related to cooling of the plutons, and thus the magnetization may be primary. The full details of the diffusion model used to draw this conclusion can be seen in the supplementary material. In the following, we focus on the heat transfer

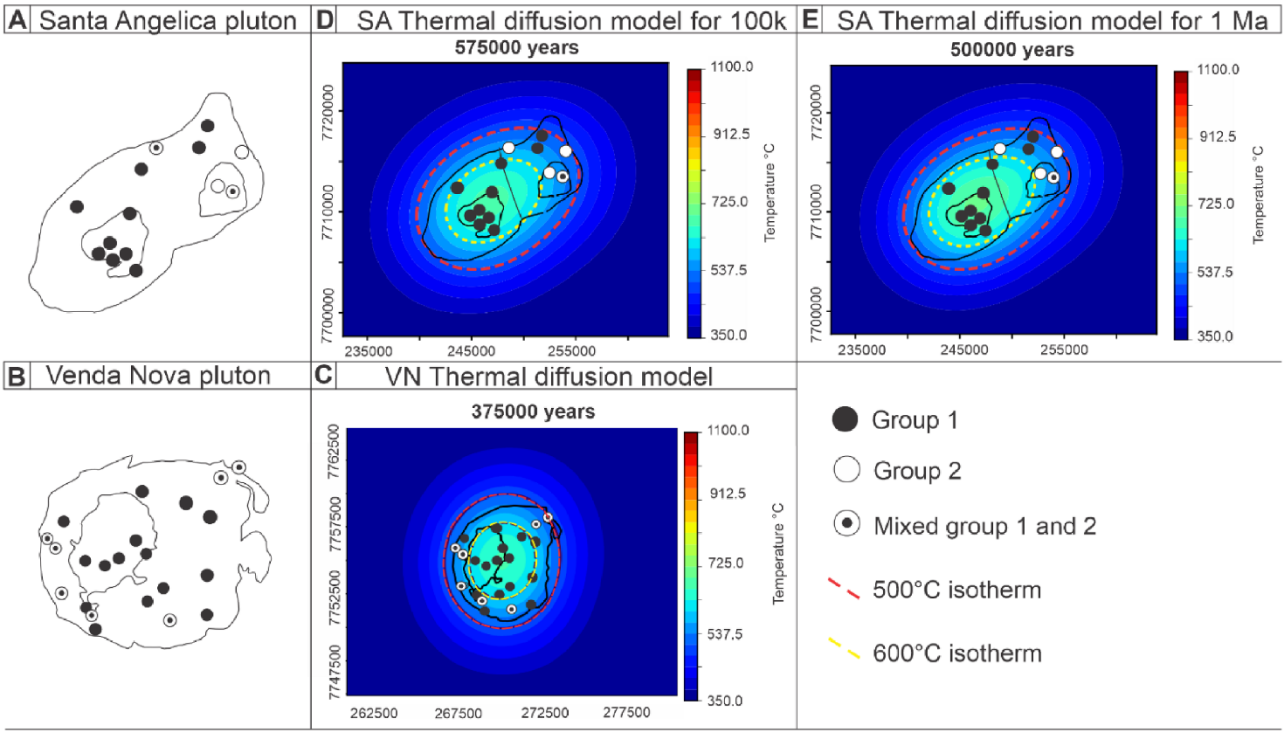

Fig. 6. Thermal diffusion model for the SA (A) and VN (B) plutons and the distribution of observed paleomagnetic polarities. (C) VN thermal diffusion model frame. (D) and (E) SA thermal diffusion model frame for 100 k years and 1 Ma, respectively.

pattern for each scenario and its relationship with the antipodal directions from each pluton (Fig. 6A, B).

In the VN pluton, heat diffusion occurs quickly through the first 100 kyr, in accordance with Fick's first law of diffusion. The gabbroic core transfers energy to the lower temperature syenite-monzonite envelope, and the highest temperature isotherms migrate from the gabbroic core to the center of the unit within 150 kyr. Before migration and re-setting of the hottest region of the pluton, the 600 °C and 500 °C isotherms are close together. Once the diffusion takes an equal spreading regime from 150 °C forward, these isotherms depart from each other. The polarities of the VN sites also exhibit a concentric distribution, with group 2 directions and mixed polarities located at the border of the pluton, and group 1 directions located at the core. Considering a range of magnetite Curie temperature (Tc) coherent with the 600 °C isotherm and 500 °C as a blocking temperature (Tb), and comparing it with the spatial distribution of the paleo-polarity at each site, it is possible to observe a coherent correlation, represented by the 375 kyr interpolation frame (Fig. 6C).

For the SA pluton, the same perspective between mafic core vs felsic envelope in the VN is observed. There is a difference in the thermal interaction between the NE and SW pluton. Both plutons are approximately coeval (Temporim et al., 2020), and our alternative thermal history scenarios (100 kyr vs. 1 Ma differences in emplacement timing) are simply formulated for the sake of comparison. The matter of which lobe would have intruded first is not relevant, because the goal is to determine whether the polarity could be related to the cooling process, and thus whether the magnetization could be primary. In the NE lobe, following 100 kyr of cooling, the 500 °C and 600 °C isotherms are close together and there is a hot core with temperatures near 900 °C. In the SW intrusion, the heat causes a funneling effect of the isotherms towards the NE lobe and, once the heat distribution is equilibrated, isotherms depart again with a much lower cooling rate. In the 1 Ma cooling scenario, the NE lobe fully passes through Tb before the intrusion of the SW lobe. The funneling effect is also present and 500 °C isotherms expands itself through a NE trend until nearly half of the NE body. Although with small differences between each other, in both scenarios the 500 °C and 600 °C isotherms are coherent with the paleo-polarity distribution in the SA - all sites that exhibit group 2 or mixed group 1 and 2 directions are located in the NE lobule and the SW lobule exhibits only group 1 directions (Fig. 6D,E).

5. Discussion

5.1. Paleomagnetic pole of the Cambrian plutons

Our paleomagnetic analysis revealed antipodal remanent magnetizations from both the SA and VN plutons, which pass a reversal test and represent indistinguishable directional populations, as attested by a CTDM test. In conjunction with our thermal diffusion models, the observed distribution of magnetic polarities is consistent with the ChRMs of the SA and VN plutons being thermoremanent magnetizations (TRMs) acquired during cooling of those plutons following their emplacement. That the A_{95} of the SA pluton is larger than that of the VN pluton is mostly likely due to their different cooling histories. According the thermal diffusion model, the amount of time to cool the SA pluton required ~600 kyr more than the VN pluton. Due the longer cooling time, SA pluton would record greater dispersion of directional data. Nevertheless, the directional dispersion of the VN data is still within the expected range for a time-averaged pole, and the presence of dual polarities strongly suggests that the dataset has averaged PSV.

Combination of the results from both plutons yields a paleomagnetic pole (hereafter 'SAVN' pole) at 332.2 °E and 4.7 °S (Table 1) for which an age of ~500 Ma is assigned based on the U-Pb analysis (Temporim et al., 2020). This pole completely satisfies all seven quality criteria proposed by Van der Voo (1990), as follows: (1) U-Pb zircon ages constraining the crystallization age of different facies within SA pluton are concordant and likely closely approximate the age of magnetization acquisition; (2) the pole was derived from a set of 309 samples (35 sites) and has adequate statistical precision (A_{95} = 4.06 and K = 68.82); (3) remanence vectors were isolated after stepwise AF and TH demagnetization, both treatments giving similar results; (4) a thermal diffusion model was used to attest that the magnetization in both plutons is most

likely a primary TRM; (5) the plutons intrude Neoproterozoic gneisses of the AO after the peak of deformation and metamorphism, as indicated by regional geochronological data and structural relations (details can be found in Temporim et al., 2020); (6) the Santa Angelica pluton presents reversals corroborated by a positive reversal test; (7) the pole does not resemble any younger paleomagnetic poles either from Gondwana or the independent South American plate after the demise of Pangea. The location of the SAVN pole is moreover similar to other ~500 Ma poles from Gondwana (see below). Meert et al. (2020) introduce a stricter (updated) R-criteria, but our new pole also completely satisfies their seven criteria. In sum, our new paleomagnetic pole may be regarded as a reference pole for the supercontinent Gondwana in Furongian time (~500 Ma).

The paleomagnetic data from this work also suggest that the Earth's magnetic field underwent at least one period of reversal during the acquisition of the remanence in these rocks. Moreover, because Gondwana was in the southern hemisphere during the early Paleozoic (see below), we may recognize the group 1 directions (directed downward) as being of reverse polarity and the group 2 directions as being of normal polarity.

5.2. Comparisons with existing constraints

Several apparent polar wander paths (APWP) have been proposed for Gondwana in latest Neoproterozoic-early Paleozoic time (e.g. Meert et al., 2003, Trindade et al., 2006, Torsvik et al., 2012, Rapalini, 2018). These paths are based on different data selection and rejection criteria, resulting in a large variety of shapes. For reference, in Fig. 7 we show the Paleozoic segment of the Gondwana APWP of Torsvik et al., 2012 (one of the larger and more recent compilations), rotated into South American (Amazonian) coordinates. More specifically, this is the 10-Myr running mean (RM) path of Torsvik et al. (2012); a variation of this path that applies a blanket inclination shallowing correction ($f = 0.6$) to all uncorrected clastic sedimentary rocks is also depicted (dashed line). Note that although this Paleozoic APWP is built from a relatively large number of poles (N = 74), they are not uniformly distributed in time. Mean poles with a white A_{95} are based on only a single entry (whereas all means with a blue A_{95} have N > 1), and the poles at 340, 420 and 430 Ma (marked by grey squares) are interpolated (i.e. N = 0).

Our new 500 Ma SAVN pole (Table 1) closely corresponds to the Furongian sector of this Gondwana APWP, and notably falls within the A_{95} of both the 500 and 510 Ma mean poles (Fig. 7). Aside from the Furongian segment, the only other part of the APWP of Gondwana that is somewhat close to the SAVN pole is the 390 Ma mean pole (10 °N, 15 °E). However, this 390 Ma mean is poorly defined, being based on only a single pole derived from sedimentary rocks that have not been corrected for inclination shallowing. Torsvik et al. (2012) discarded this pole in favor of an interpolated result (grey 390 Ma pole in Fig. 7), and, notably, application of an assumed inclination shallowing correction of $f = 0.6$ results in a shift of the original mean toward this interpolated position.

Although the comparison of the SAVN pole against the reference Gondwana APWP of Torsvik et al. (2012) is instructive, it is also important to directly compare it against similarly aged individual poles. This is especially important given the fact that the Cambrian Epoch 2-Tremadocian segment of the Gondwana APWP of Torsvik et al. (2012) is near-entirely dominated by results from Eastern Gondwana. Of the 19 late Cambrian Epoch 2-Tremadocian (530–480 Ma) poles from Gondwana in that compilation, ten are from Australia, four are from

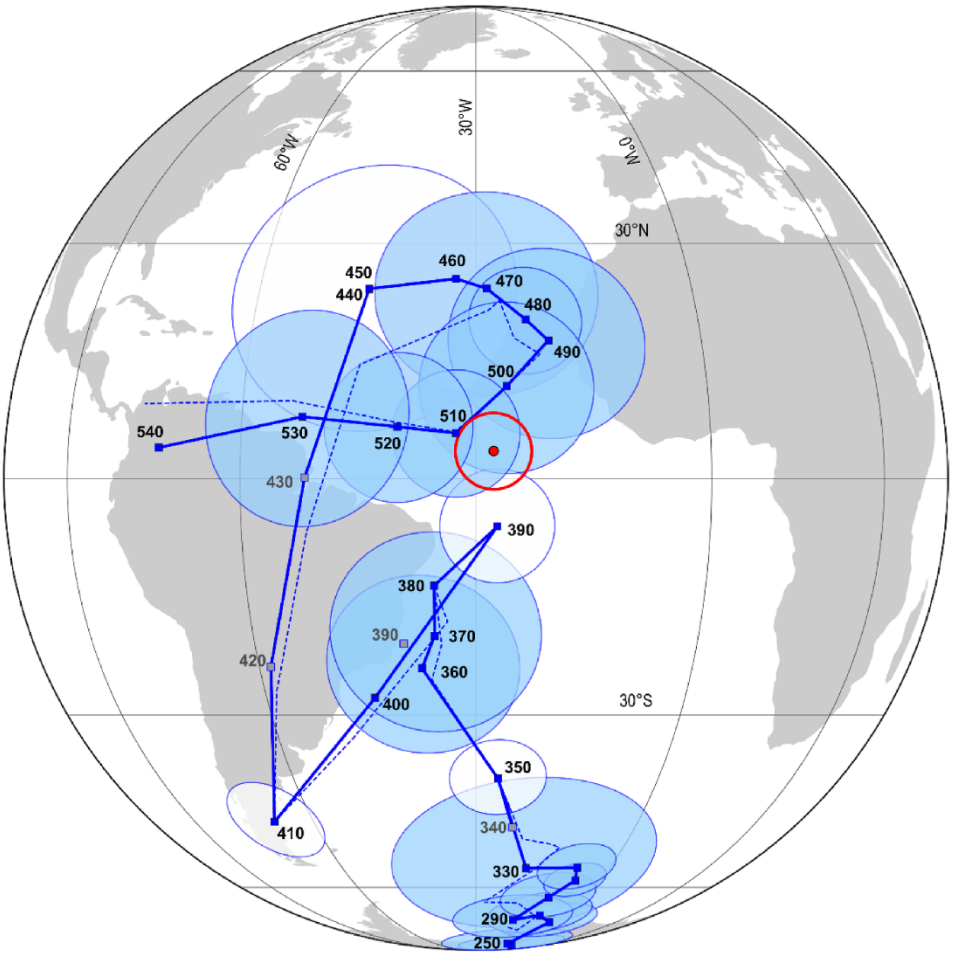

Fig. 7. Apparent Polar Wander Path (APWP) of Gondwana (Torsvik et al., 2012) in Amazonian coordinates. The solid line represents the 10-Ma running mean path (using a 20-Ma window) without correction for potential inclination shallowing; the dashed line is the same path after inclination shallowing correction with a blanket value of f = 0.6. Mean poles with a white A95 are based on only a single entry (whereas all blue A95s have N > 1). Mean poles denoted by grey squares (430, 420, 390 and 340 Ma) were determined by interpolation from the neighboring mean poles. The SAVN pole is shown in red.

Antarctica and two are from Madagascar. The remaining three poles are from southeastern Africa and the Rio de la Plata Craton, and there are no Cambrian Epoch 2-Tremadocian (poles from Congo-São Francisco. We therefore compiled Cambrian Epoch 2-Tremadocian (525–480 Ma) poles from Western Gondwana (Table 2) to evaluate the position of SAVN with respect to coeval poles from more closely neighboring regions. In addition to the aforementioned poles from Torsvik et al. (2012), our compilation includes three poles from Congo-São Francisco and two poles from the Pampean Orogen. We sought poles with Q > 4, but retained the singular pole from Rio de la Plata with Q = 3.

In Fig. 8 we plot the SAVN pole against these other poles after rotating them to South American (Amazonian) coordinates, following the reconstruction parameters of Torsvik et al. (2012) (see Table 2). Among these poles, the results from the Piquete Formation (PI, ca.500–490 Ma, D'Agrella Filho and Pacca, 1986) and Juiz de Fora (JF, ca.510–500 Ma, D'Agrella-Filho et al., 2004) are the most directly comparable to SAVN, in being the only other poles from the Araçuaí orogen. JF lies only ~6° from SAVN and its A_{95} overlaps the SAVN mean, whereas the PI pole falls ~15° from SAVN and is statistically distinct from it. Although the first-order similarity among these pole positions is noteworthy, an interpretation of their differences is inhibited by the fact that the PI and JF poles are derived from metamorphic rocks whose ages are not precisely determined. Aside from the PI and JF poles, the only other similarly aged pole from Congo-São Francisco is the Itabaiana pole (IT, ca. 525 Ma; Trindade et al. 2006), which falls ~34° from SAVN. However, given that the best-estimated ages of these poles differ by ~25 Ma, their separation could be simply explained by plate motion at a rate on the order of 15 cm yr^{-1}.

Looking beyond Congo-São Francisco, the Cambrian Epoch 2 pole from Rio de la Plata (SI) falls close to (~6° from) the SAVN mean, but is associated with large spatial and temporal uncertainties. A Tremadocian pole from South Africa (Graafwater, GF pole) also falls ~10° from the SAVN mean, whereas the Cambrian Epoch 2 Ntonya Ring pole (NR) from southeastern Africa lies ~24° away. Observing that the latter falls close to the IT pole (Trindade et al. 2006), its position is again possibly reflective of the Cambrian Epoch 2 drift of Western Gondwana. These results are thus consistent with a general coherence between Congo-São Francisco, Rio de la Plata and southern Africa by Cambrian Epoch 2 time. In contrast, two Furongian-Tremadocian poles from the Pampean orogen fall more than 25° from SAVN and the other Furongian-Tremadocian poles from Western Gondwana (Franceschinis et al. 2020). Their pole positions are also significantly offset from the coeval mean poles of the APWP of Torsvik et al. (2012). Their anomalous positions could be interpreted as evidence of a significant younger displacement of the Pampean orogen with respect to greater Gondwana (e.g. Spagnuolo, et al., 2012), although the available geological evidence strongly opposes such a scenario (Rapela et al., 2007; Ramos et al., 2010). This remains an outstanding problem.

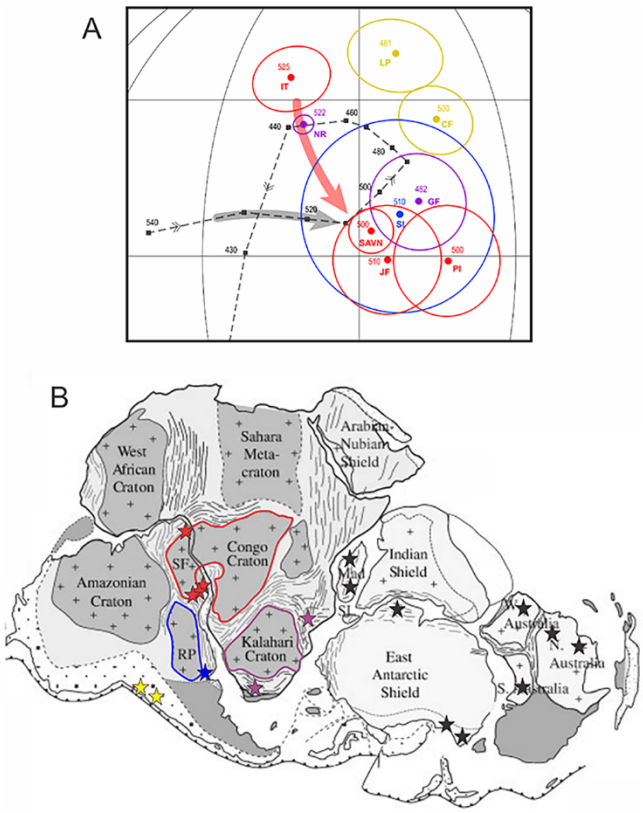

Fig. 8. Cambrian Epoch 2 to Tremadocian paleomagnetic poles of Gondwana. A) Poles rotated to the Amazon coordinates following the reconstruction parameters of Torsvik et al. (2012). The collection includes poles from Congo-São Francisco craton (red), Pampean Orogen (yellow), Rio de la Plata (blue), and Southeastern Africa (purple). All information and references of the poles can be seen in the Table 2 of this work. APWP for Gondwana between 540 and 430 is represented in dashed gray lines (Torsvik et al., 2012). B) Gondwana map (Gray et al., 2007) with localities from Western Gondwana in colorful stars and localities from Eastern Gondwana in black stars.

A key observation from these comparisons is that our ~500 Ma SAVN pole agrees well with the Gondwana APWP of Torsvik et al. (2012), which is dominated by Eastern Gondwana data, and with individual Terreneuvian-Tremadocian poles from Western Gondwana. This implies that Eastern and Western Gondwana must have been approximately coherent at least by this time. In contrast, the slightly older Cambrian poles (Cambrian Epoch 2) from Western Gondwana (IT and NR) appear to diverge from the Terreneuvian and Cambrian Epoch 2 trend of the

Table 2
Selected paleomagnetic poles for Gondwana between 525 and 480 Ma. Q = Quality Factor (Van der Voo, 1990); A95 = 95% confidence ellipse; Lat/Lon = Pole Latitude/Longitude; Age in Ma.

Code	Formation	Q	Plat	Plon	A_{95}	Age	EP	Reference
Congo-São Francisco								
SAVN	Santa Angelica/Venda Nova plutons, Araçuai Orogen	7	4.7	332.2	4.1	500	–	This work
PI	Piquete Formation, Araçuai Orogen	4	−0.8	346.5	10.2	500	–	D'Agrella Filho and Pacca (1986)
JF	Juiz de Fora Complex	4	−0.6	335.2	10	510	–	D'Agrella-Filho et al. (2004)
IT	Itabaiana Dikes, Borborema Province	6	−34.9	134.6	7.3	525	–	Trindade et al. (2006)
Rio de la Plata								
SI	Sierra de las Animas volcanic Complex	3	5.9	338.1	18.1	510	[8.4, 111.2, −2.6]	Sanchez-Bettucci et al. (2002)
Pampean Orogen								
LP	La Pedrera Formation	5	38.3	340.4	8.8	485–477	[7.7, 298.5, 3.3]	Rodríguez Piceda et al. (2018)
CF	Campanario Formation	7	23.6	346.5	7	514–485	[7.7, 298.5, 3.3]	Franceschinis et al. (2020)
Southeastern Africa								
GF	Graafwater Formation, Cape Province	6	28	14	9	482.5	[50.0, −32.5, −55.1]	Bachtadse et al. (1987)
NR	Ntonya Ring Structure, Malawi	5	27.5	344.8	1.9	522	[50.2, 327.7, −55.0]	Briden (1968)

Gondwana APWP of Torsvik et al. (2012) (Fig. 8), implying that Western and Eastern Gondwana may have still been moving relative to one another immediately prior to mid-Cambrian time (Robert et al. 2018).

6. Conclusions

Paleomagnetic analysis was conducted on the post-collisional Santa Angélica and Venda Nova plutons (~500 Ma) from the southern portion of the Araçuaí orogen (AO) in SE Brazil. The results of this analysis isolated a characteristic magnetization likely carried by PSD/SD magnetite grains, as determined from a series of rock magnetic experiments. The population of magnetic directions from both plutons are associated with two groups which, for the Santa Angelica pluton, are demonstrated to be antipodal. A thermal diffusion model was used to demonstrate that the magnetization in both plutons is consistent with a primary thermoremanent magnetization, acquired in the midst of a field reversal. The SAVN pole computed from the pooled magnetic results (4.7° N, 332.2° E, N = 35, A_{95} = 4.06 and K = 68.82) does not resemble any younger paleomagnetic poles either from Gondwana or the independent South American plate after the demise of Pangea. In sum, this pole completely satisfies all seven quality criteria proposed by Van der Voo (1990), as well as the stricter (updated) R-criteria proposed by Meert et al. (2020).

The SAVN pole closely corresponds to the Miaolingian-Furongian sector of the Gondwana APWP (Torsvik et al., 2012), and notably falls within the A_{95} of both the 500 and 510 Ma mean poles of that path. The Terreneuvian-Tremadocian segment of the Gondwana APWP of Torsvik et al. (2012) is near-entirely dominated by results from Eastern Gondwana. The few poles from Western Gondwana are from southeastern Africa and the Rio de la Plata Craton, and there are no Terreneuvian-Tremadocian poles from Congo-São Francisco; our new pole therefore provides a critical new constraint from this block in the core of Western Gondwana. In comparing our SAVN pole with individual Cambrian Epoch 2-Tremadocian poles from Western and Eastern Gondwana, we may conclude that Eastern and Western Gondwana appear to share a common population of paleomagnetic poles by Furongian time (~500 Ma), but that there are paleomagnetic indications of strong motions between those blocks in earlier Terreneuvian-Cambrian Epoch 2 time.

CRediT authorship contribution statement

F.A. Temporim: Conceptualization, Methodology, Investigation, Visualization, Writing - original draft. **U.D. Bellon:** Methodology, Software, Formal analysis, Investigation, Visualization. **M. Domeier:** Conceptualization, Methodology, Visualization, Supervision. **R.I.F. Trindade:** Methodology, Supervision, Project administration, Funding acquisition. **M.S. D'Agrella-Filho:** Investigation. **E. Tohver:** .

Declaration of Competing Interest

The authors declare that they have no known competing financial interests or personal relationships that could have appeared to influence the work reported in this paper.

Acknowledgments

The authors would like to express their gratitude to the Laboratório de Paleomagnetismo (USPmag) of the Universidade de São Paulo. This works was funded by grants of Fundação de Amparo à Pesquisa do Estado de São Paulo (FAPESP, #2016/06114-6, #2017/11672-0 and #2019/18892-1). We also thank the fellowship provided by the Coordenação de Aperfeiçoamento de Pessoal de Nível Superior – Brasil (CAPES), Finance Code 001. This work was also supported by the Research Council of Norway (RCN) through its Centres of Excellence funding scheme, project 223272 (CEED) and through RCN project 250111.

Appendix A. Supplementary data

Supplementary data to this article can be found online at https://doi.org/10.1016/j.precamres.2021.106212.

References

Alkmim, F.F., Marshak, S., Pedrosa-Soares, A.C., Peres, G.G., Cruz, S.C.P., Whittington, A., 2006. Kinematic evolution of the Araçuaí-West Congo orogen in Brazil and Africa: nutcracker tectonics during the Neoproterozoic assembly of Gondwana. Precambr. Res. 149 (1-2), 43–64. https://doi.org/10.1016/j.precamres.2006.06.007.

Bachtadse, V., Van der Voo, R., Hälbich, I.W., 1987. Paleomagnetism of the western Cape Fold belt, South Africa, and its bearing on the Paleozoic apparent polar wander path for Gondwana. Earth Planet. Sci. Lett. 84 (4), 487–499.

Bayer, B., Schimidt-Thomé, R., Weber-Diefenbach, K., Horn, H.A., 1987. Complex concentric granitoid intrusions in the coastal mobile belt, Espírito Santo, Brazil: the Santa Angélica Pluton – an example. Geologische Rubdschau. 76 (2), 357–371. https://doi.org/10.1007/BF01821080.

Briden, J.C., 1968. Paleomagnetism of the Ntonya Ring Structure, Malawi. J. Geophys. Res. 73 (2), 725–733.

Clauser, C., 2009. Heat transport processes in the earth's crust. Surv. Geophys. 30 (3), 163–191. https://doi.org/10.1007/s10712-009-9058-2.

D'Agrella-Filho, M.S., Raposo, M.I.B., Egydio-Silva, M., 2004. Paleomagnetic study of the Juiz de Fora Complex, SE Brazil: implications for Gondwana. Gondwana Res. 7 (1), 103–113. https://doi.org/10.1016/S1342-937X(05)70309-9.

D'Agrella Filho, M.S., Pacca, I.G., 1986. Paleomagnetism of metamorphic rocks from the Piquete region – Ribeira Valley, Southeastern Brazil. Rev. Brasileira de Geofis. 4, 79–84.

De Campos, C.M., Medeiros, S.R., Mendes, J.C., Pedrosa-Soares, A.C., Dussin, I., Ludka, I. P., Dantas, E.L., 2016. Cambro-Ordovician magmatism in the Araçuaí Belt (SE Brazil): snapshots from a post-collisional event. J. S. Am. Earth Sci. 68, 248–268. https://doi.org/10.1016/j.jsames.2015.11.016.

Deenen, M.H.L., Langereis, C.G., van Hinsbergen, D.J.J., Biggin, A.J., 2011. Geomagnetic secular variation and the statistics of palaeomagnetic directions. Geophys. J. Int. 186 (2), 509–520. https://doi.org/10.1111/j.1365-246X.2011.05050.x.

Dunlop, D.J., Argyle, K.S., 1991. Separating multidomain and single-domain-like remanences in pseudo-single-domain magnetites (215–540 nm) by low-temperature demagnetization. 96, 2007-2017. https://doi.org/10.1029/90JB02338.

Franceschinis, P.R., Rapalini, A.E., Escayola, M.P., Rodríguez Piceda, C., 2020. Paleogeographic and tectonic evolution of the Pampia Terrane in the Cambrian: New paleomagnetic constraints. Tectonophysics 779, 228386. https://doi.org/10.1016/j.tecto.2020.228386.

Fisher, R., 1953. Dispersion on a sphere. Proc. R. Soc. London. 217 (1130), 295–305. https://doi.org/10.1098/rspa.1953.0064.

Granade de Araujo, C.E., Rubatto, D., Hermann, J., Cordani, H.G., Caby, R., Basei, M., 2014. Ediacaran 2,500-km-long synchronous deep continental subduction in the West Gondwana Orogen. Nat. Commun. 5 (1), 5198. https://doi.org/10.1038/ncomms6198.

Gray, D.R., Foster, D.A., Meert, J.D., Goscombe, B.D., Armstrong, R., Trouw, R.A.J., Passchier, W., 2007. A Damara orogen perspective on the assembly of southwestern Gondwana. Geol. Soc. 294, 257–278. https://doi.org/10.1144/SP294.14.

Kirschvink, J.L., 1980. The least-squares line and plane and the analysis of palaeomagnetic data. Geophys. J. Int. 62 (3), 699–718. https://doi.org/10.1111/gji.1980.62.issue-310.1111/j.1365-246X.1980.tb02601.x.

Koymans, M.R., Langereis, G.C., Pastor-Galán, D., van Hinsbergen, D.J.J., 2016. Paleomagnetism.org: An online multi-platform open source environment for paleomagnetic data analysis. Comput. Geosci. 93, 127–137. https://doi.org/10.1016/j.cageo.2016.05.007.

Kröner, A., Stern, R.J., 2005. Africa: Pan-African Orogeny. In: Encyclopedia of Geology. Elsevier, Oxford, pp. 1–13.

Li, Z.-X., Evans, D.A.D., Halverson, G.P., 2013. Neoproterozoic glaciations in a revised global palaeogeography from the breakup of Rodinia to the assembly of Gondwanaland. Sedim. Geol., 294, pp. 219–232.

Meert, J.G., Van der Voo, R., 1997. The assembly of Gondwana 800–550 Ma. J. Geodyn. 23, 223–235. https://doi.org/10.1016/S0264-3707(96)00046-4.

Meert, J.G., Nédélec, A., Hall, C., 2003. The stratoid granites of central Madagascar: paleomagnetism and further age constraints on neoproterozoic deformation. Precambr. Res. 120 (1-2), 101–129. https://doi.org/10.1016/S0301-9268(02)00161-4.

Meert, J.G., Pivarunas, A.F., Evans, D.A.D., Pisarevsky, S.A., Pesonen, L.J., Li, Z.X., Elming, S.A., Miller, S.R., Zhang, S., Salminen, J.M., 2020. The magnificent seven: a proposal for modest revision of the Van der Voo (1990) quality index. Tectonophysics 790, 228549. https://doi.org/10.1016/j.tecto.2020.228549.

Mendes, J.C., De Campos, C.M.P., 2012. Norite and charnockites from the Venda Nova Pluton, SE Brazil: intensive parameters and some petrogenetic constraints. Geosci. Front. 3 (6), 789–800. https://doi.org/10.1016/j.gsf.2012.05.009.

Pedrosa-Soares, A.C., Wiedemann-Leonardos, C.M., 2000. Evolution of the Araçuaí belt and its connection to the Ribeira Belt, Eastern Brazil. In: U.G. Cordani, E.J. Milani, A. Thomaz Filho, D.A. Campos (Eds.) Tectonic Evolution of South America. São Paulo, SBG, 265-285.

Pedrosa-Soares, A.C., Noce, C.M., Wiedemann, C.M., Pinto, C.P., 2001. The Araçuaí-West Congo orogen in Brazil: An overview of a confined orogen formed during

Gondwanland assembly. Precambr. Res. 110, 307–323. https://doi.org/10.1016/S0301-9268(01)00174-7.
Pedrosa-Soares, A.C., De Campos, C.P., Noce, C.M., Silva, L.C., Novo, T., Roncato, J., Medeiros, S., Castaneda, C., Queiroga, G., Dantas, E., Dussin, I., Alkmim, F.F., 2011. Late Neoproterozoic-Cambrian granitic magmatism in the Araçuaí orogen (Brazil), the eastern Brazilian Pegmatite province and related Mineral resources. In: Sial, A. N., Bettencourt, J.S., De Campos, C.P., Ferreira, V.P. (Eds.), Granite related Ore Deposits, 350. Geological Society, London, pp. 25e51. Special Publications.
Ramos, V.A., Vujovich, G., Martino, R., Otamendi, J., 2010. Pampia: a large cratonic block missing in the Rodinia supercontinent. J. Geodyn. 50 (3-4), 243–255. https://doi.org/10.1016/j.jog.2010.01.019.
Rapalini, A.E., 2018. Assembly of Western Gondwana reconstruction based on paleomagnetic data. In S. Siegesmund, M. Basei y P. Oyantzabal (Eds.), Geology of Southwest Gondwana. Springer-Verlag, pp. 3-18. DOI: 10.1007/978-3-319-68920-3_1.
Rapela, C.W., Pankhurst, R.J., Casquet, C., Fanning, C.M., Baldo, E.G., González-Casado, J.M., Galindo, C., Dahlquist, J., 2007. The Río de la Plata craton and the assembly of SW Gondwana. Earth Sci. Rev. 83 (1-2), 49–82. https://doi.org/10.1016/j.earscirev.2007.03.004.
Robert, B., Greff-Lefftz, M., Besse, J., 2018. True polar wander: a key indicator for plate configuration and mantle convection during the Late Neoproterozoic. Geochem. Geophys. Geosyst. 19 (9), 3478–3495. https://doi.org/10.1029/2018GC007490.
Rodríguez Piceda, C., Franceschinis, P.R., Escayola, M.P., Rapalini, A.E., 2018. Paleomagnetismo del Grupo Santa Victoria en la sierra de Mojotoro, Salta: aportes a la reconstrucción paleogeográfica de Pampia en el Paleozoico Temprano. Revista de la Asociacion Geologica Argentina. 4, 518–532. https://doi.org/10.1016/j.psep.2018.03.001.
Sanchez-Bettucci, L., Rapalini, A.E., 2002. Paleomagnetism of the Sierra de Las Animas Complex, southern Uruguay: its implications in the assembly of western Gondwana. Precambr. Res. 118, 243–265.
Schmidt-Thomé, R., Weber-Diefenbach, K., 1987. Evidence for frozen-in magma mixing in Brasiliano calc-alkaline intrusions. The Santa Angélica pluton, southern Espírito Santo, Brazil. Revista Brasileira de Geociências 17, 498–506.
Spagnuolo, C.M., Rapalini, A.E., Astini, R.A., 2012. Assembly of Pampia to the SW Gondwana margin: A case of strike-slip docking?. Gondwana Research. 21? 406–421. doi: 10.1016/j.gr.2011.02.004.
Tauxe, L., Butler, R.F., Van der Voo, R., Banerjee, S.K., 2010. Essentials of Paleomagnetism. University of California Press, California.
Tedeschi, M., Novo, T., Pedrosa-Soares, A., Dussin, I., Tassinari, C., Silva, L.C., Gonçalves, L., Alkmim, F., Lana, C., Figueiredo, C., Dantas, E., Medeiros, S., De Campos, C., Corrales, F., Heilbron, M., 2016. The Ediacaran Rio Doce magmatic arc revisited (Araçuaí-Ribeira orogenic system, SE Brazil). J. S. Am. Earth Sci. 68, 167–186. https://doi.org/10.1016/j.jsames.2015.11.011.
Temporim, F.A., Trindade, R.I.F., Tohver, E., Soares, C.C., Gouvêa, L.P., Egydio-Silva, M., Amaral, C.A.D., Souza Jr., G.F., 2020. Magnetic Fabric and Geochronology of a Cambrian "Isotropic" Pluton in the Neoproterozoic Araçuaí Orogen. Tectonics. 39 (6), e2019TC005877. https://doi.org/10.1029/2019TC005877.
Tohver, E., D'agrella Filho, M.S., Trindade, R.I.F., 2006. Paleomagnetic record of Africa and South America for the 1200–500 Ma interval, and evaluation of Rodinia and Gondwana assemblies. Precambr. Res. 147, 193–222.
Tohver, E., Cawood, P.A., Rossello, E.A., Jourdan, F., 2012. Closure of the Clymene Ocean and formation of West Gondwana in the Cambrian: evidence from the Sierras Australes of the southernmost Rio de la Plata craton, Argentina. Gondwana Res. 21 (2-3), 394–405. https://doi.org/10.1016/j.gr.2011.04.001.
Trindade, R., Dagrellafilho, M., Epof, I., Britoneves, B., 2006. Paleomagnetism of Early Cambrian Itabaiana mafic dikes (NE Brazil) and the final assembly of Gondwana. Earth Planet. Sci. Lett. 244 (1-2), 361–377. https://doi.org/10.1016/j.epsl.2005.12.039.
Torsvik, T.H., Cocks, R.M., 2011. The Palaeozoic palaeogeography of central Gondwana. Geological Society, London, Special Publications, 357, 137-166. https://doi.org/10.1144/SP357.8.
Torsvik, T., Cocks, L., 2016. Earth History and Palaeogeography. Cambridge: Cambridge University Press. doi:10.1017/9781316225523.
Torsvik, T.H., Van der Voo, R., Preeden, U., Mac Niocaill, C., Steinberger, B., Doubrovine, P.V., van Hinsbergen, D.J.J., Domeier, M., Gaina, C., Tohver, E., Meert, J.G., McCausland, P.J.A., Cocks, L.R.M., 2012. Phanerozoic polar wander, palaeogeography and dynamics. Earth Sci. Rev. 114 (3-4), 325–368. https://doi.org/10.1016/j.earscirev.2012.06.007.
Van der Voo, R., 1990. The reliability of paleomagnetic data. Tectonophysics 184, 1–9. http://hdl.handle.net/2027.42/28314.
Vandamme, D., 1994. A new method to determine paleosecular variation. Phys. Earth Planet. Inter. 85 (1-2), 131–142. https://doi.org/10.1016/0031-9201(94)90012-4.
Wilson, T.J., Grunow, A.M., Hanson, R.E., 1997. Gondwana assembly: the view from Southern Africa and East Gondwana. J. Geodyn. 23 (3-4), 263–286. https://doi.org/10.1016/S0264-3707(96)00048-8.